Temperature Control of Porous Media Burner Based on Advanced Reduced Instruction Machine -PID Algorithm and Embedded Processor

Jingtao Guan
School of Computer Science and Engineering, Guangdong Ocean University, Yangjiang 529500, China
Email: gjt_gdou@163.com

Abstract: Against the backdrop of the rapid development of metal smelting processes, the requirements for reaction temperature control are gradually increasing, and the temperature control system for porous media burners based on advanced simplified instruction embedded processors has been developed. In this burner, the fuel is heated using a porous medium for conduction, which generates various complex data during operation and can overload conventional algorithms. To reduce the difficulty of algorithm operation, this study introduced an adaptive database into the proportional integral differential algorithm to classify data and establish a load balancer in the advanced reduced instruction algorithm, which is convenient for embedded processing of large amounts of data. To avoid the algorithm falling into local optima, this study merged the digital output module with it during temperature control to generate a fusion system. Finally, this study conducted experiments on the Porbu dataset and compared it with three systems such as generalized predictive control to verify the superiority of the fusion system. The temperature control accuracy of the four systems was 99.7%, 97.2%, 96.1%, and 93.5%, respectively, indicating that the efficiency of the fusion system performs the best among the four systems. The energy consumption of this system was 0.038kW * h, which performs best among the four systems. The experimental results indicate that the fusion system proposed in this study has the strongest performance and is suitable for precise temperature control of porous media burners.

Keywords: Porous media; Advanced Reduced Instruction Algorithm; PID algorithm; Adaptive database; Temperature control; Embedded processing; Load balancer; Digital output module

1. Introduction

With the increasing demand for metallurgical industry products, porous media burners, as an efficient combustion equipment, have received widespread attention in the research of temperature control technology [1-2]. The interior of a porous medium burner (PMB) is composed of porous media, which can provide a larger combustion surface area and make the combustion effect of the fuel more uniform [3-4]. Due to the presence of rough surfaces in the medium, the device undergoes complex heat conduction during operation, resulting in the loss of fuel heat [5]. The Proportional Integral Differential (PID) system is a control system that controls the temperature inside the burner by adjusting the fuel and oxygen supply [6]. However, the PMB generates too much data during operation, and the search domain of the conventional PID algorithm is too narrow, which can cause confusion during operation. International experts have proposed the method of setting up an adaptive database (AD) within it to classify a wide range of data. But this method is only applicable to data within small collection boxes, and for large-scale datasets, this method is prone to falling into local optima at runtime [7]. To solve this problem, this study inputs a Load Balancer (LB) in an embedded system based on the Advanced Reduced Instruction Machine (ARM) architecture, and establishes a Digital Output Module (DOM) in it to filter the

output data and generate a fusion system (ARM-PIDLB). The main contributions of this study are three points. Firstly, the algorithm is used to convert temperature information into electrical signals, allowing for more accurate analysis of the temperature of the burner. Secondly, the temperature control methods of PMBs have been enriched through new methods. Finally, the utilization rate of the substances in the burner is improved through the PID algorithm. The research is mainly divided into four parts. Part 1 mainly analyzes and summarizes the application fields of current advanced simplified instruction algorithms and the methods applied to burner temperature control. The second part mainly constructs a remote temperature control system for burners based on PID algorithm. Part 3 is an analysis of the performance of the fusion system proposed in the study. The fourth part is a summary of this study and proposes shortcomings. This study aims to improve the temperature control capability of PMBs, thereby promoting the purity improvement of metal smelting technology.

2. Related Works

With the rapid development of temperature control technology, research on temperature control based on porous media burners is increasing. Ding et al. believed that when automatic guided vehicles are applied in the industrial field, most control strategies do not consider temperature control. So they used PID algorithm to combine the dual wheel chassis model with fast navigation technology, while considering both axle chassis and proportional integral micro control. In terms of data support, they used navigation technology to provide control strategies, and their experimental environment contains unfavorable scenarios and operating conditions to prove their strategies. This method not only comprehensively improved temperature control performance, but also had stability and robustness in terms of results [8]. Considering that the bearing temperature of wind turbines needs to be controlled, which is susceptible to nonlinear effects, Wang et al. proposed a suspension strategy based on PID predictive control to improve the interference ability of dynamic response. They first established a mathematical model, and then used the method of combining PID with bearings to design a floating air gap tracking outer ring controller. This method had better robustness compared to existing control strategies and could achieve smooth and reliable operation [9]. Due to the fact that the commonly used international method is embedded processing, which has an advantage in processing large amounts of data, Liu et al. documented the limitations of the level set data processing method and considered it a challenging task. They corrected the extracted information based on embedded processing methods, first embedding saliency information into the level set method, which had favorable quality and made the background prominent. By combining edge information, the processed data would be more accurate, and their methods would be more efficient, fast, reliable, and have strong robustness [10].

With the development and growth of PID algorithm, research on temperature control using algorithms is gradually being carried out. Liu et al. conducted a two-dimensional numerical simulation study on the combustion process in a PMB. They optimized the wall impact model and introduced interaction mechanisms to adapt the model to temperature control under different conditions. They believed that the flame propagation speed was proportional to the joint effect parameters at the same equivalence ratio. At the same time, the effects of fuel injection quantity and preheating temperature on spray combustion were also analyzed. As the reaction progressed, the rate of increase in flame area gradually decreased [11]. Mohammadi et al. conducted numerical simulations of the performance of the burner and used the additional energy of porous solids to enrich the control equation system, extending chemical transport to multi-step mechanisms. This numerical model mainly validated existing benchmark experiments, while

taking into account both classical contributions and turbulent dissipation, effectively controlling the local entropy generation rate and air coefficient caused by mixing. Their PMB had excellent temperature control performance [12]. Omidi et al. conducted experiments on the temperature control performance of metal porous burners. They created surface flames in porous media while observing the performance of the burner, and studied thermal efficiency and pollutant emissions by changing factors such as thermal power and equivalence ratio. With the increase of thermal power generation, the emissions of nitric oxide were also increasing. Under all measurement conditions, when the equivalence ratio was 0.8 and the thermal power was 100kW, the emission of carbon monoxide was the lowest, and at this time, the temperature control performance of the burner was the best [13].

The research of numerous experts has proven that there are various methods for studying temperature control, and ARM is also widely used in various fields. However, there is still little research on combining this algorithm with temperature control of porous media burners. To fill the research gap in this section, this study creatively applies the ARM algorithm to the temperature control of PMBs, hoping to promote the development of the metal smelting industry.

3. Construction of a PMB Control System based on ARM Embedded Processor

In order to improve the combustion efficiency of the burner and ensure the safety and reliability of the combustion process, this study is based on an ARM architecture embedded system to establish a control system for the PMB, which is used to manage the operation of the PMB. The system precisely controls it by integrating sensors, actuators, and PID control algorithms. Through the high-performance and low-power characteristics of ARM embedded processors, the system can collect and process sensor data in real-time, and make precise adjustments based on control algorithms.

3.1 Embedded processor combining ARM and PID automatic control

Embedded processor is a type of microprocessor specifically designed for ARM systems, which has high-performance characteristics and is suitable for various application fields [14]. PID, as a commonly used automatic control algorithm, can adjust the output of the system to the desired reference value. The PID algorithm adjusts the output signal based on the current error size and rate of change to achieve system responsiveness. The combination of both embedded processors can achieve efficient real-time systems. The ARM processor is used to collect sensor data and execute computational controllers. The PID algorithm can communicate on the ARM processor through peripheral interfaces, as shown in equation (1).

$$U_t(x) = k_0 * \int w(t)\,dt + k_1 * \left[dw(t) \right] / (dt) + k_2 * w(t) \quad (1)$$

In equation (1), $w(t)$ represents the input data of the algorithm regulator. k_0 is its input bias. k_1, k_2 are the operating deviation and output deviation [15], respectively. This processor implements various components of the PID algorithm through programming, and its characteristics enable it to calculate output in real-time and respond quickly to system changes. The flexibility and programmability of ARM processors make them suitable for different control needs, and can meet the requirements of real-time and reliability. The embedded processor that combines ARM and PID automatic control (PID-AC) is a powerful tool that can play an important

role in applications, as shown in Figure 1.

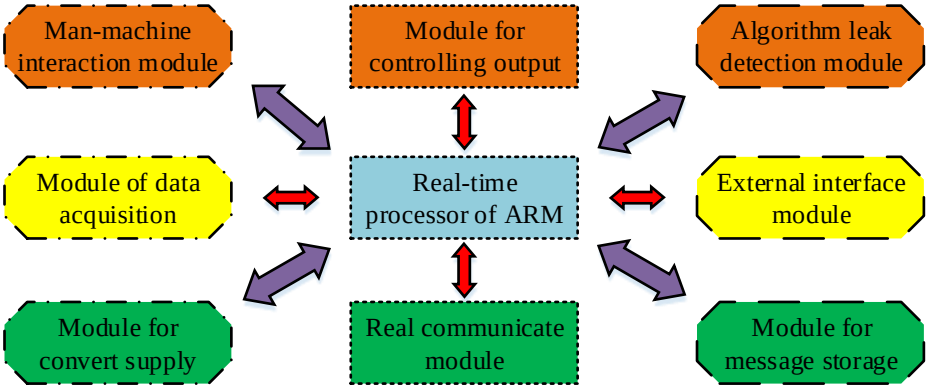

Figure 1 Embedded processor combined with ARM and PID-AC

Figure 1 shows the processor architecture with both ARM and PID-AC effects. The microprocessor adopts a reduced instruction set computer architecture, which can provide excellent performance under low power consumption conditions and is customized according to application requirements, with universality from single core processors to multi-core processors. This processor supports multiple operating systems, making it an ideal choice for developing embedded systems. The PID-AC algorithm is used to adjust the current error value and calculate the control signal through three parts, which follow equation (2) during operation.

$$G_s = -\frac{\alpha_1 + \alpha_2}{\beta} * \left[\frac{1}{s*(\alpha_1 + \alpha_2)} + \frac{s*\alpha_1*\alpha_2}{\alpha_1 + \alpha_2} + 1 \right] \quad (2)$$

In equation (2), the gain of the algorithm in the proportional phase is denoted as β, and its time constant in integration and differentiation is represented by α_1, α_2. s represents the time regulator of the algorithm. The time deviation of this method depends on the specific requirements of the control system, which is only based on the size of the error. This method is suitable for simple control systems, which can lead to steady-state errors in complex systems. Due to the fact that in addition to the proportional term, this method also needs to consider the integration of errors. In order to reduce steady-state errors while avoiding overshoot, this study applies constant treatment to the differential of errors based on proportional and integral terms. And fuzzy logic is used to calculate the control signal, thereby defining the membership function of fuzzy rules, as shown in equation (3).

$$\begin{cases} \int Su(x)dx = \sum_{k=1}^{n} Cy * Su(k) \\ dSu(k)/dk = \left[Su(k) - Su(k-1) \right]/t \end{cases} \quad (3)$$

In equation (3), Cy represents the expected steady-state error of the algorithm. The output values randomly extracted from the data at the t-th moment are represented by $Su(k)$. The total time of data collection is recorded as k. The embedded processor combining ARM and PID-AC can achieve precise regulation of various substances. The hardware selection criteria include interfaces and actuators. Implement PID control algorithm on ARM processor to adjust the working status of the actuator in real-time based on sensor data and set target values. To quickly

process these complex sensor data, this study introduced AD into the ARM-PID algorithm, which can effectively monitor the database load, as shown in Figure 2.

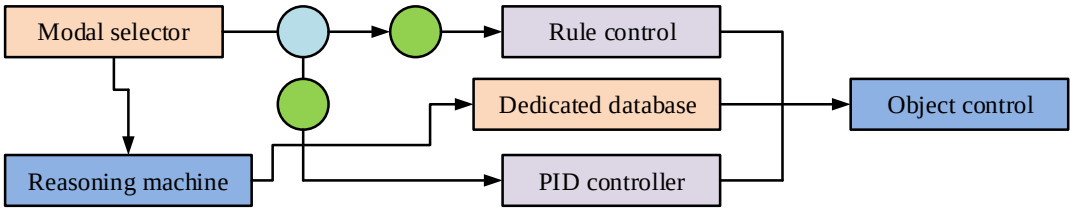

Figure 2 Architecture diagram of ARM-PID algorithm with AD

Figure 2 shows the ARM-PID algorithm with AD added. To achieve adaptive addition of database functionality, this study uses monitoring tools to monitor the load of the database in real-time. This method can understand the performance status of the database and whether it is necessary to increase the database capacity to generate a fusion algorithm (ARM-PIDLB). Based on the database load situation, this study considers increasing the time required for database capacity. When the database load exceeds the threshold, the method studied automatically triggers database expansion [16]. If the database capacity has reached the upper limit, the data will be migrated to a larger database, which is achieved by backing up and restoring the data. To achieve real-time monitoring of data, this study conducted sampling detection on the data, as shown in equation (4).

$$Sa_k = Su(k)*\left(K_p - K_t\right) + K_t * \sum_{t=1}^{T}\left(K_t - K_{t-1}\right) \quad (4)$$

In equation (4), Sa_k represents the theoretical output value of the database. K_p is the theoretical maximum load of the database, and the actual load is denoted as K_t. When the database load is too high, this method adds LB to the database to distribute requests to multiple database instances to meet the growing data demand and maintain the performance and availability of the database. After increasing the database capacity, this study monitors the load situation of the database for performance optimization. This step includes index optimization and cache optimization, with the aim of improving the response speed of the database and thereby achieving the function of adaptively increasing the database. The overload problem of the database uses load balancing technology to distribute requests, as shown in equation (5) below.

$$\overline{Ba(k)} = \sum_{k=0}^{k} Sa_k + \chi_s * \left[Ba(k) - Ba(k-1)\right] \quad (5)$$

In equation (5) above, $Ba(k)$ represents the database load at the sampling time, and its mean is denoted as $\overline{Ba(k)}$. The error during data transmission is represented by χ_s, which is related to the inherent properties of LB. This machine is a device responsible for distributing traffic, which can evenly distribute traffic to multiple servers to ensure that each computing resource can effectively process requests. LB balances different factors to improve the performance and response speed of the entire system. When computing resources fail, they have the ability to reallocate. So this study added LB mechanism to ARM-PID, and the process is Figure 3.

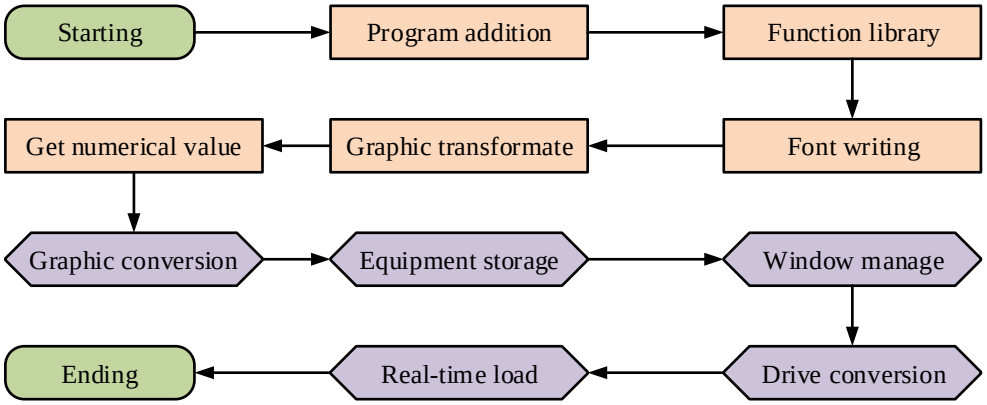

Figure 3 Workflow diagram after adding LB mechanism in ARM-PID

Figure 3 shows the ARM-PID process after adding LB functionality. This study adds more computing resources to help the system cope with the increasing traffic [17]. The function of LB is traffic distribution, which simplifies the complexity of system management. It can intelligently schedule based on real-time server status. During scheduling, the parameter changes between servers follow equation (6).

$$\Delta\delta_1 = \phi_1 * (\varepsilon_1 - \varepsilon_0) + \phi_2 * (\gamma_1 - \gamma_0) + \sum_{x=1}^{X} \varphi_x * \phi_x \quad (6)$$

In equation (6), the server scheduling coefficient during incremental calculation is denoted as ϕ_1. $\varepsilon_1, \varepsilon_0$ represent the increased flow and the original system flow, respectively. ϕ_2 is the traversal coefficient between server layers, which is related to manual experience γ_1 and rule design γ_0. The total number of layers of the server is represented by X. φ_x represents the theoretical output of the system at this time. This method can be connected to a debugger for reliability testing of the system. This study will deploy the designed system into actual devices, and the deployment method is shown in formula (7). At the same time, the performance optimization and parameter adjustment of the device are carried out to achieve higher operating efficiency.

$$\eta_p = \frac{2\phi_x * \left[(\iota_a - \iota_b)/2 \right]}{\iota_a + \iota_b} \quad (7)$$

In equation (7), the domain of the dataset is denoted as η_p. ι_a and ι_b represent the continuity and discontinuity points, respectively. This method can accurately calculate the input values of the ARM-PIDLB controller while preserving the real-time nature of the data. Due to the precise control of the burner being the focus of this study, this algorithm can improve the operational stability of the burner. So the communication interface can achieve remote monitoring, thereby achieving the best combustion effect and energy utilization rate.

3.2 Design of PMB temperature control system integrating ARM-PIDLB

In the system design, considering the environmental friendliness during the working process, this study first debugged temperature and oxygen sensors. Simultaneously calculating the fuel supply parameters of the porous medium in the integrated actuator ensures real-time control of the

temperature state of the burner. To achieve data interaction between the system and external devices, this study added an integrated communication interface. In addition, for the safe operation of the system, measures have been added to implement fault alarms [18]. In this study, the PMB temperature control system design of ARM-PIDLB should comprehensively consider the integration of software and construct their structure as shown in Figure 4.

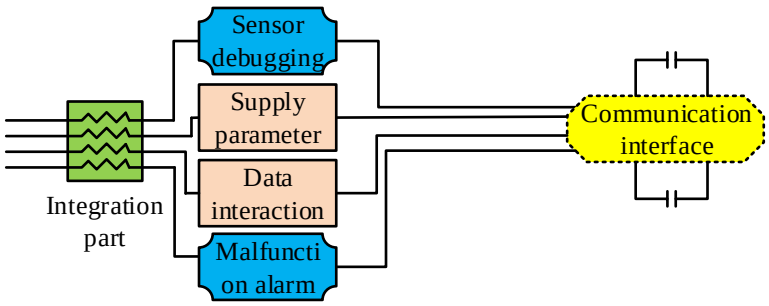

Figure 4 Software integration in the design of temperature control system of PMB based on ARM-PIDLB

In Figure 4, this study first establishes the core control unit of the system to receive temperature data from sensors and generate control instructions based on the ARM-PIDLB algorithm. Then there is the connection of the data collection node, which is responsible for patrolling various areas of the burner and transmitting data to the main control node. For the control instructions sent by the main control node, this study achieves parallel control of burner temperature. Due to the collected temperature data being in a pending state, a data storage node was set up to achieve distributed data storage. The relationship between the collected temperature data is equation (8).

$$Qc = Ew * \frac{d\kappa_0}{d\lambda} + En * \frac{d\kappa_1}{d\lambda} + \frac{|\kappa_0 - \kappa_1|}{Rx} \quad (8)$$

In formula (8), the heat release of PMB during time λ is denoted as Qc. The specific heat capacities of the outer and inner walls of the device are represented by Ew, En, and their instantaneous temperatures are recorded as κ_0, κ_1. The coil resistance of the burner is Rx. The signals for this study include analog signals and digital signals. The temperature sensor converts temperature into electrical signals and serves as an analog signal conditioning circuit. In this process, it will be converted into a digital signal and converted into digital form for digital filtering. The temperature signal after signal processing can be used to control the temperature of the burner. As the burner continues to operate, the coil resistance continues to increase, and the signal measurement in the circuit changes [19]. To achieve effective control of signal measurement, this study considers its frequency controllability to be strong and performs calculations on it, as shown in equation (9).

$$Hz = Qc * \sum_{i=1}^{I} Ad_i * \frac{Vo_i}{Ia_i} \quad (9)$$

In equation (9), the changing factor of signal conversion is denoted as Ad_i. The coil voltage and current here are represented by Vo_i and Ia_i. I represents the total number of coils, which is related to the real-time strength of the electrical signal. This study records changes in electrical signals to monitor the signal quality of ARM-PIDLB. This is of great significance for temperature

control of the burner and can help solve network problems. The electrical signal data studied was recorded using a signal collector, and software tools were used to control hardware devices and analyze the electrical data. The process is Figure 5.

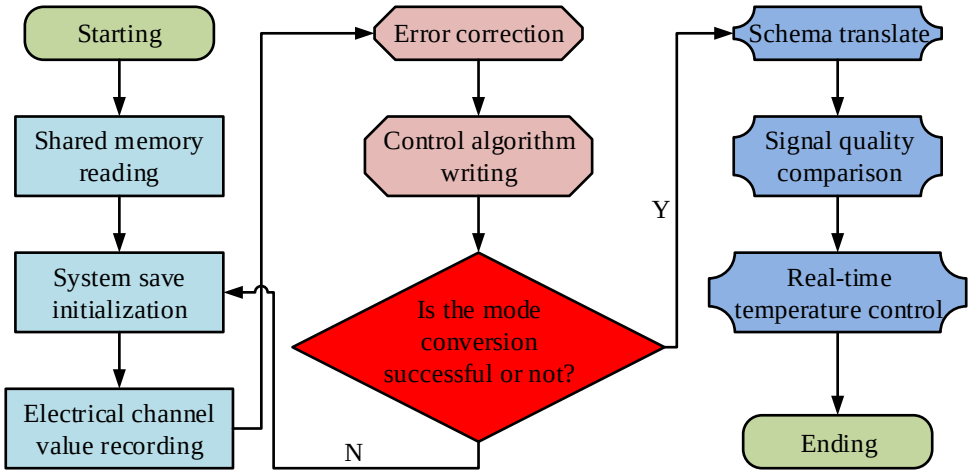

Figure 5 Flowchart for analyzing electrical data by software tools to control hardware devices

Figure 5 is a method of connecting temperature and electrical signal data. This study conducted electrical signal data collection in the ARM-PIDLB system. To meet this requirement, this study installed temperature sensors in the burner, with a total of 42 thermocouples. These sensors filter and linearly process weak electrical signals, and then convert analog electrical signals into digital signals. The instrument used in this step is an analog-to-digital converter, which can input digital signals into the computer. The data acquisition system communicates with the computer through an interface and transmits temperature data to the control system for further control operations. During the process of system communication, the electrical signal will undergo slight changes, described by equation (10).

$$CH_e = Qc^{-1} * \sum_{i=0}^{T_1} \left(Us_i / Tr_i \right) \quad (10)$$

In equation (10), the propagation amplitude of the electrical signal is denoted as CH_e. The frequencies of its sawtooth wave and tree wave are represented by Us_i and Tr_i, respectively. During system operation, in order to convert electrical signals into analog outputs, a DOM is set up in the ARM-PIDLB system. It has multiple output channels and independently sets output values in each channel to control multiple tasks simultaneously. DOM has adjustable output values, which can adjust the voltage or current range of the output according to the preset temperature, and its amplitude of change is equation (11).

$$\begin{cases} Ul_1 = Ul * \left[\left(\nu - 1 \right) + o_1 * \varpi_1 + \Delta CH_e \right] \\ Ul_2 = Ul * \left[\left(\nu - 1 \right) + o_2 * \varpi_2 + \Delta CH_e \right] \end{cases} \quad (11)$$

In equation (11), the voltage between the two main roads is denoted as Ul_1, Ul_2. o_1, o_2 is the current flowing between them, and their resistances are ϖ_1, ϖ_2, respectively. Ul, ν represents the voltage and current of the branch, respectively. Connecting to the system through an interface and set output value parameters for configuration and control functions. In conventional applications,

this device usually needs to work offline. This study aims to design an offline fuzzy processing module for temperature control of fuzzy burners. It can extract specific features for pattern matching and apply filters to convert input electrical signals into temperature values. The workflow is Figure 6.

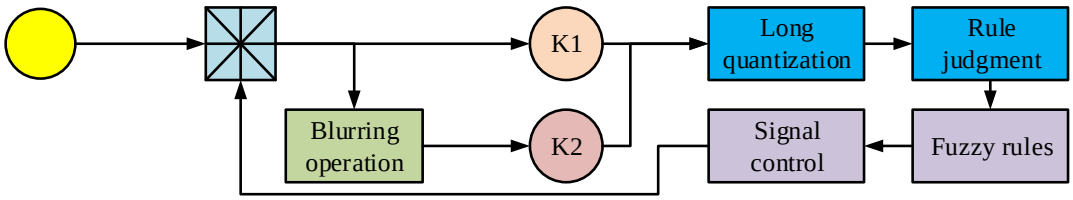

Figure 6 Fuzzy decision flow of burner in off-line state

Figure 6 is an explanation of the fuzzy decision method for the ARM-PIDLB system in offline situations. This method uses the weighted average of the electrical signal sampling points input by the fuzzy kernel and the temperature in adjacent times to obtain the electrical signal at the current time, making the temperature control result smoother. Set adjustable parameters in the offline fuzzy processing module to handle temperatures exceeding predetermined values. This module has real-time processing capabilities to reduce noise or interference, thereby improving the efficiency of PMB. For fuzzy control, communication and synchronization between tasks are required, and the synchronization method is as follows (12).

$$\begin{cases} un_1 = Ul * \sum_{i=1}^{k} \left(\theta_i * \vartheta_i + un_0 \right) \\ \theta_i = 0.5 * \left(\vartheta_i - \vartheta_{i-1} \right) + 1 \end{cases} \quad (12)$$

In equation (12) above, the system preset temperature is denoted as un_0. un_1 represents the real-time temperature of the burner. θ_i, ϑ_i is the measured value and variation value of the system at the current time. The change from the previous moment is represented by ϑ_{i-1}. After information synchronization, the ARM-PIDLB system will obtain a temperature control signal, which will be fed back to the burner to achieve closed-loop temperature control [20]. Set up a feedback loop during the signal feedback process. The macroscopic manifestation of the feedback loop on the burner device is an electric valve, which can start working when the temperature does not meet expectations and adopts the rules shown in equation (13).

$$\Delta Si = \frac{\theta_i * \left| \sigma_1 - \sigma_0 \right|}{25 * Fe - 1} \quad (13)$$

In equation (13), the preset temperature is denoted as σ_0. The real-time temperature of the burner is represented by σ_1. Fe represents the working condition of the feedback loop, which is related to the sample collection efficiency of the collector. For the substances in the burner, in order to achieve precise temperature control of PMB, a sample temperature collection device was added to the equipment, and its activity flow during sample collection is Figure 7.

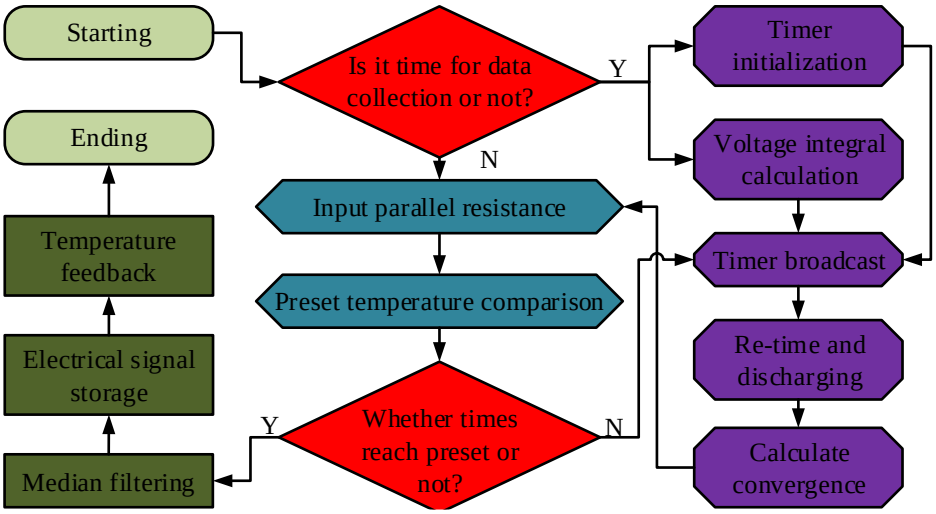

Figure 7 Temperature acquisition device in ARM-PIDLB system

Figure 7 introduces the working process of the temperature acquisition device during PMB operation. Firstly, the sampling period of the system is set, and the voltage signal is used to power the integrator. When the sampling time on the timer reaches the preset value, the system will input the resistance value of the parallel resistor and compare it with the set temperature. When the expected number of samples in the burner is achieved, this study performs median filtering on the collected data and resets the electrical signal to provide real-time temperature feedback in the PMB. During this process, the propagation path of the control voltage is denoted by equation (14).

$$Cv_s = \frac{\varsigma}{\tau d + 1} \quad (14)$$

In equation (14), ς is the time constant of PMB, and the lag time of the system is represented by τd. In actual PMB sampling, the sampling environment is a cross compilation environment. It is a condition used to compile executable programs of different systems, which can optimize the development of embedded systems. In this environment, cross compilers can serve as a toolchain to compile source code. The result obtained from this toolchain is the machine code of the burner, which is used to link the necessary files of the temperature control program. The system involves environment variables and compilation option parameters when configuring the PMB structure. This study aims to improve the precision of temperature control by building a cross compilation environment and implementing an application program suitable for temperature control on the burner operating system, as shown in equation (15).

$$Qb = Fu * Sh * \frac{d\Delta\omega}{dt} + TTco * TTa * \Delta\omega \quad (15)$$

In equation (15), the time interval is denoted as $\Delta\omega$. The fuel volume of the burner is represented by Fu. The specific heat capacity of the fuel is denoted as Sh. $\Delta\omega$ represents the heating time of the burner, and its heat transfer constant is expressed in $TTco$. TTa is the contact area between the fuel and PMB. Due to the fact that the interior of the heater can be regarded as a closed system and the pressure inside is close to atmospheric pressure, the error in the experimental environment can be ignored. This study only needs to calculate the heat loss of the heater based on formula (8). This method can control environmental errors while also having strong robustness in temperature extraction of porous medium heaters.

4. Characterization of temperature Control Performance of ARM-PIDLB System in PMB

In order to explore the temperature control performance of the ARM-PIDLB system in PMB, this study conducted experiments on the Porbu dataset. This dataset contains a total of 200 burners with different operating voltages, including various heating methods for fuels such as coal and natural gas. Therefore, this study conducted temperature control performance analysis on them under the same conditions of controlling external air pressure.

4.1 Analysis of temperature control capability of embedded processors based on ARM

Due to the limited number of data contained in the Porbu dataset, this study divided the dataset into a training set and a testing set in a ratio of 2:3. Before the experiment, the experimental parameters and equipment were first set to ensure the effectiveness of the experiment, as shown in Table 1.

Table 1. Experimental parameters and equipment setting of temperature control for embedded processor based on ARM

Device type	System parameters or software
Language	Easy Chinese
Computer chip	Intel i6 CPU
System memory	256G*2
Working time of the system	10:06:31
Sampling frequency	48Hz
Execution method	Matlab R2021a
Data set	Porbu
Operating system	Windows XP
Liquid crystal controller	SSD2119 3.5TFT
Pin level	0100PSO
Electric work of burner	330W
Electric coupler	PC260

After setting the parameters according to Table 1, this study conducted temperature control performance experiments on the ARM-PIDLB system. To verify the efficiency of the system, temperature control experiments were conducted on ARM system, Spotted hyena Algorithm (SH) system, and Generalized Predictive Control (GPC) system simultaneously. The experimental results are shown in Figure 8.

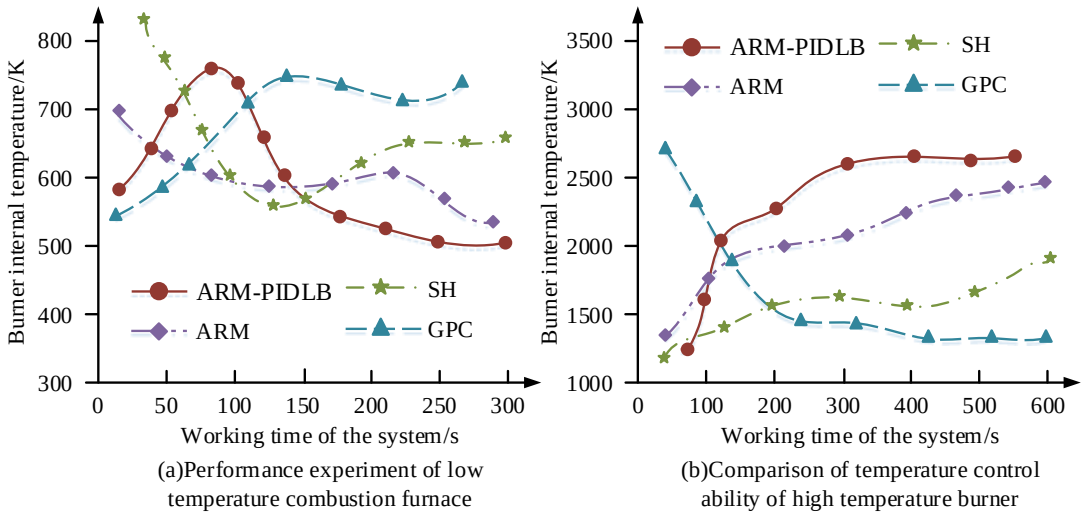

Figure 8 Comparison of temperature control ability of the system to the burner at different temperatures

In Figure 8 (a), the temperature of PMB gradually approaches the preset value. Under the preset temperature of 625K, the heating time of the ARM-PIDLB system is 45 seconds. This value performs best among the four systems, with temperature correction times of 68s, 87s, and 132s for ARM, SH, and GPC systems, respectively. This indicates that in the comparison of temperature control performance of low-temperature PMB, the ARM-PIDLB system has the strongest temperature control ability. Figure 8 (b) shows the temperature control performance experiment in a high-temperature environment, where the operating times of the four systems are 84s, 125s, 167s, and 159s, respectively. This is because the thermodynamic properties of high-temperature burners are stable, making it difficult to change their heating state. For heating pots of different sizes, experimental analysis was also conducted, and the results are shown in Figure 9.

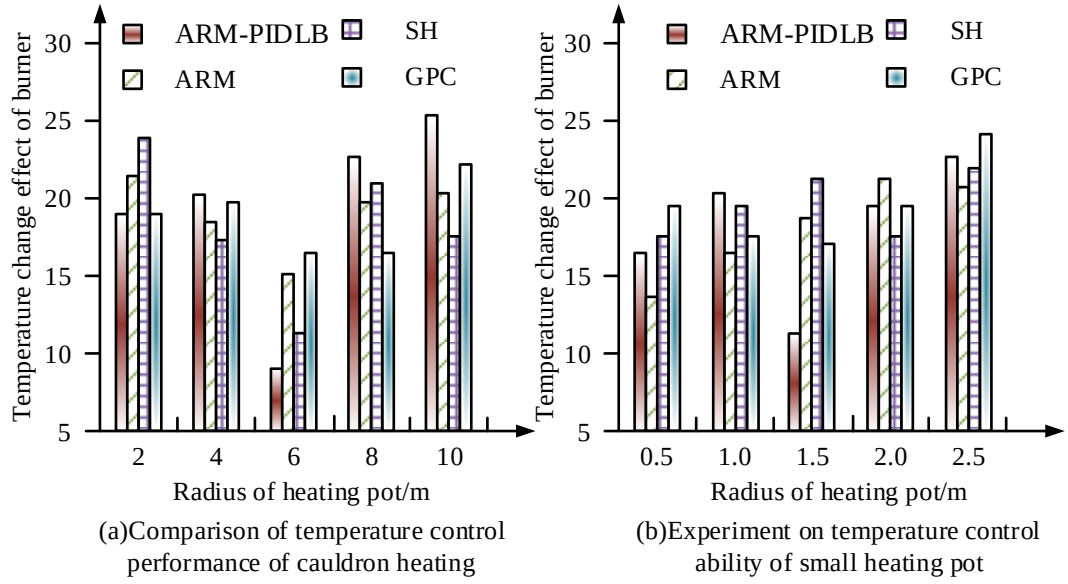

Figure 9 Comparison of temperature control ability of four systems with different sizes

In Figure 9 (a), when the operating area of the heating pot is 6, the temperature control

capabilities of the four systems in the burner are optimal, with their relative control peaks of 8, 14, 12, and 19, respectively. This indicates that when the temperature control performance of the ARM-PIDLB system is optimal, the heat transfer area needs to be controlled around 6. In Figure 9 (b), the optimal temperature control environment for the proposed fusion system is 1.5, with a control peak of 11. The values for the other three systems are 18, 24, and 21, respectively. This indicates that the temperature control performance of the ARM-PIDLB system is optimal when the volume fraction of the heating pot is 1.5 and 6. To verify the universality of the system, 40 experiments were conducted in this study, and the experimental results are shown in Figure 10.

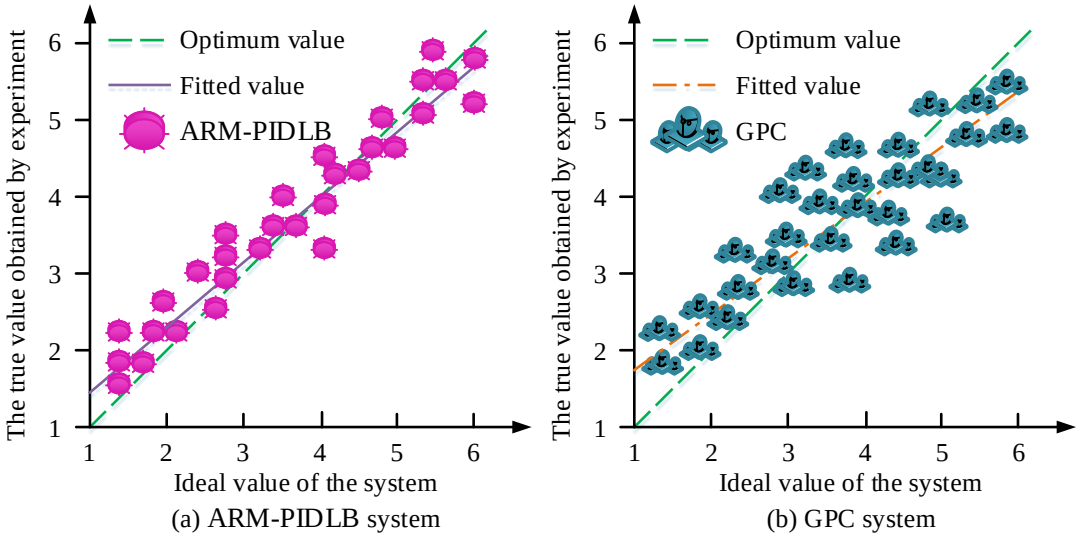

Figure 10 Relationship between Graphic Size and Printing Materials

Figure 10 is a comprehensive experiment conducted on the research system. Forty experiments have shown that the experimental results of the research system are closer to the true values, with a linear fit of 0.9998. The linear fit of the GPC system is relatively different, with a value of 0.9827. The experimental results indicate that the ARM-PIDLB system has stability in temperature control of PMB. However, this result can only be applied to the external environment of the burner, and the performance of the system still needs to be experimentally verified for changes in internal parameters of the PMB.

4.2 Experimental verification of temperature control in PMB using ARM-PIDLB fusion system

This experiment first designs variables for PMB and integrates ARM-PIDLB with them. Then, different temperature target values are set for temperature control experiments. During the experiment, the fusion system will change the temperature based on real-time temperature data, and the experimental results will be used to analyze the temperature control effect of the system in PMB. This study first controls the operating voltage of the system to be the same, and then analyzes the temperature control ability of the ARM-PIDLB system in low and high voltage environments. The experimental results are shown in Figure 11.

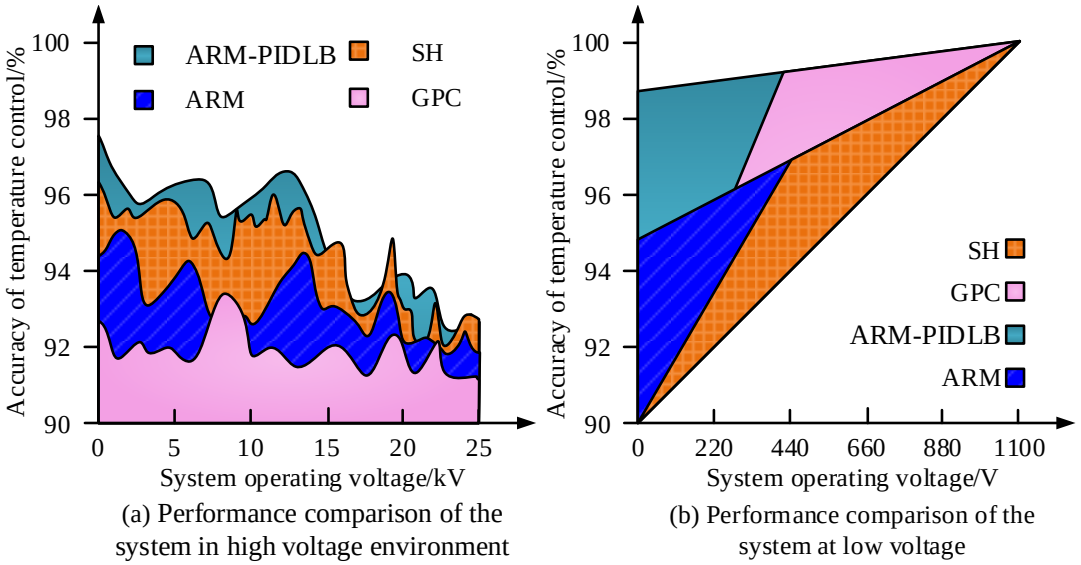

(a) Performance comparison of the system in high voltage environment

(b) Performance comparison of the system at low voltage

Figure 11 Experiment control ability of ARM-PIDLB system under different voltages

In Figure 11 (a), the control accuracy of all four systems shows a decreasing trend in high-pressure environments. When the voltage reaches 13kV, the ARM-PIDLB system has the highest accuracy of 97.4%. The accuracy rates of ARM, SH, and GPC systems are 96.1%, 94.5%, and 92.6%, respectively. This indicates that in high-pressure environments, the fusion system has the highest robustness. In Figure 11 (b), when the system operates in a low voltage environment, the accuracy of all four systems is proportional to the voltage. When the voltage is 425V, their accuracy reaches its peak, and the accuracy of the four systems is 99.7%, 97.2%, 96.1%, and 93.5%, respectively. This indicates that the efficiency of the fusion system is related to the burner voltage and performs better at low voltage. To determine the accuracy of this method, an experiment was conducted to measure the F1 value, as shown in Figure 12.

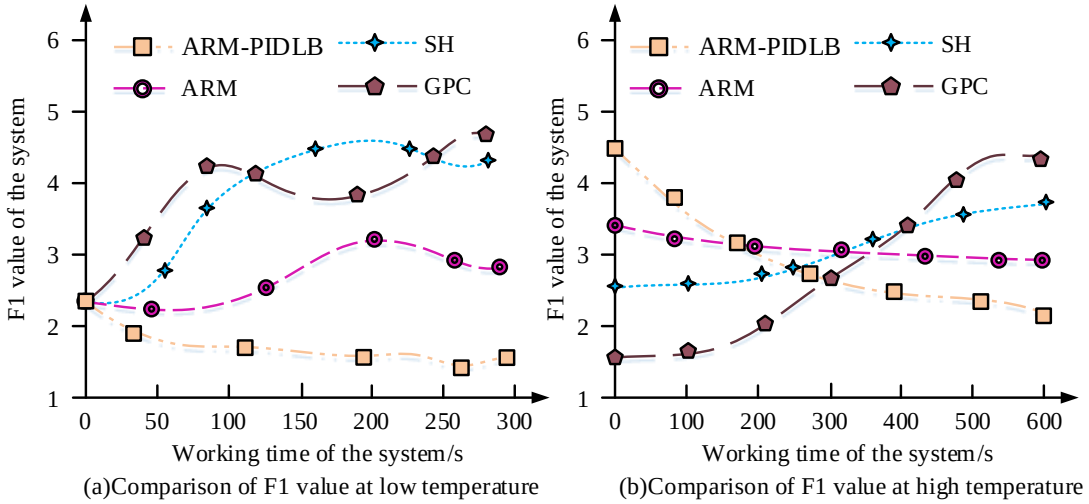

(a)Comparison of F1 value at low temperature

(b)Comparison of F1 value at high temperature

Figure 12 Measurement experiment of F1 value of four systems

Figure 12 compares the F1 values of four systems. As the working time of the system accumulates, the F1 values of all four systems show an upward trend. The experimental results of

ARM-PIDLB, ARM, SH, and GPC systems in low-temperature environments are 1.4, 2.5, 3.1, and 5.6, respectively. At high temperatures, the F1 values of the four are 2.1, 2.8, 3.6, and 4.7, respectively. The results indicate that the ARM-PIDLB system performs optimally in different temperature environments, and its system state is better at low temperatures than at high temperatures. Figure 13 shows the results of evaluating their performance.

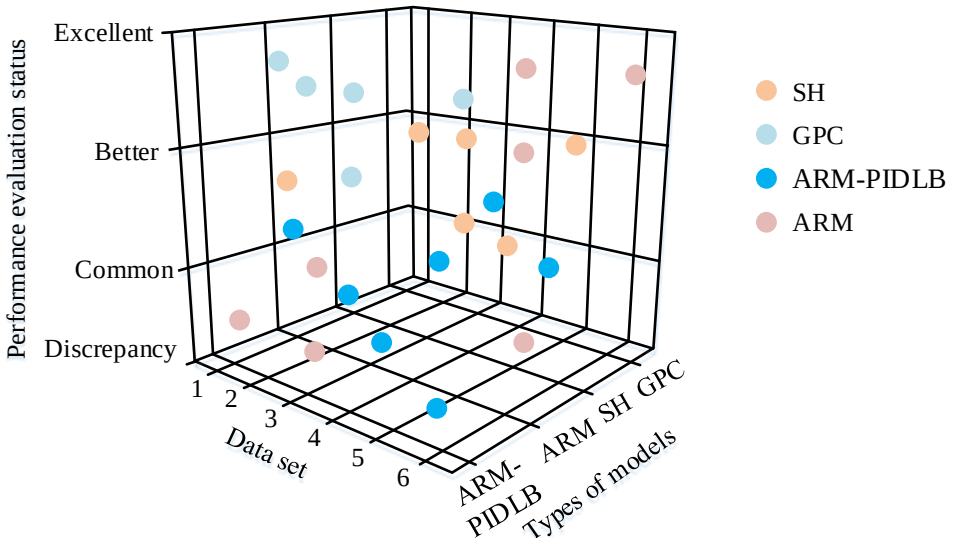

Figure 13 Experimental results of performance evaluation of four systems

In Figure 13, when the temperature control time of ARM-PIDLB and ARM systems is 17 and 21 minutes, the temperature of PMB reaches stability, with temperature values of 375 and 401K, respectively. Under the preset temperature of 370K, this result indicates that the proposed fusion system has stronger temperature control ability, while the burner temperatures controlled by the SH and GPC systems are 217K and 265K, respectively. This indicates that under the same internal parameters of the system, the experimental data of the ARM-PIDLB system is globally optimal. To conduct experiments on the energy loss performance of the system, this study conducted temperature control in the same PMB, and the experimental results are shown in Figure 14.

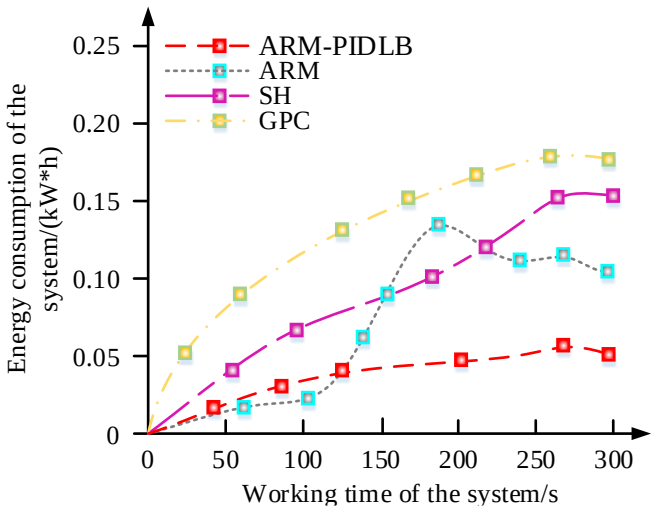

Figure 14 Working Time Diagram of the Algorithm Before and After Optimization

In Figure 14, the energy consumption of the four systems is directly proportional to the operating time. Although the proposed fusion system had a higher power consumption than the ARM system before reaching 126 seconds, the energy consumption of the ARM-PIDLB system remained stable and was the lowest among the four systems, with a value of 0.038kW * h. At this time, the energy consumption of the other three systems is 0.097, 0.136, and 0.157kW * h, respectively, indicating that the system has the best energy savings. The experimental results indicate that the ARM-PIDLB system proposed in the study has the strongest PMB temperature control ability and is suitable for improving the heat value utilization rate of fuel.

5. Conclusion

Against the backdrop of the rapid development of metal purification processes, the demand for output products is gradually increasing, and temperature control during the reaction process is receiving attention. To accurately control it, a fusion system (ARM-PIDLB) was established in this study. To verify the effectiveness and universality of the system, this study conducted experiments on the Porbu dataset and compared the experimental results with those of ARM, SH, and GPC systems. When the preset temperature is 625K, the heating time of the ARM-PIDLB system was 45 seconds, which performed best among the four systems. The working time of the system in high-temperature environments was 84 seconds, indicating that the ARM-PIDLB system had temperature adaptability. When the voltage was 13kV, the accuracy of ARM-PIDLB, ARM, SH, and GPC systems was 97.4%, 96.1%, 94.5%, and 92.6%, respectively. When the voltage was 425V, their accuracy results were the best, with values of 99.7%, 97.2%, 96.1%, and 93.5%, respectively. This indicates that the ARM-PIDLB system can respond promptly to changes in operating voltage. Under the preset temperature of 370K, the temperature control results of the four systems are 375, 401, 217, and 265K, respectively. This indicated that the experimental data of the ARM-PIDLB system performed best when the internal parameters of the system were the same. For temperature control at the same time, the energy consumption of ARM-PIDLB, ARM, SH, and GPC systems was 0.038, 0.097, 0.136, and 0.157 kW * h, respectively. The above data indicated that the proposed ARM-PIDLB system not only achieved optimal temperature control capability, optimal control effect, and maximum economic benefits, but also had the widest application capability, suitable for precise temperature control of PMB. However, due to the excessive number of coil winding, excitation current will be generated during the experiment, causing errors in the experimental results. This issue will be improved with the upgrade of the equipment. This is also the next step in the research direction.

Reference

[1] Y. Guo, Z. Mustafaoglu, and D. Koundal, “Spam Detection Using Bidirectional Transformers and Machine Learning Classifier Algorithms,” Journal of Computational and Cognitive Engineering., vol. 2, no. 1, pp. 5-9, May. 2022. DOI:10.47852/bonviewJCCE2202192.

[2] G. Kumari, S. Rao, and B. Rao, “Flower pollination-based K-means algorithm for medical image compression,” International Journal of Advanced Intelligence Paradigms, vol. 18, no. 2, pp. 171-192, Sep. 2021. DOI:10.1504/IJAIP.2021.112903.

[3] X. Chen, X. Yang, H. Pang, and Y. Ou, “Design and implementation of an optical module based on an improved incremental proportional integral differential algorithm,” Journal of Intelligent & Fuzzy Systems, vol. 40, no. 4, pp. 6287-6294, Apr. 2021. DOI：

10.3233/JIFS-189465.

[4] A. Abed, Z. Rashid, F. Abedi, S. Zeebaree, M. Sahib, A. Mohamad, G. Redha, R. Maher, A. Abdulkareem, and I. Ibraheem, “Trajectory tracking of differential drive mobile robots using fractional-order proportional-integral-derivative controller design tuned by an enhanced fruit fly optimization,” Measurement and Control, vol. 55, no. 4, pp. 209-226, Jun. 2022. DOI:10.1177/00202940221092134.

[5] M. Ünver, M. Olgun, and E. Türkarslan, “Cosine and cotangent similarity measures based on Choquet integral for Spherical fuzzy sets and applications to pattern recognition,” Journal of Computational and Cognitive Engineering., vol. 1, no. 1, pp. 21-31, September. 2022. DOI：10.7315/CDE.2020.056.

[6] E. Set, B. Elik, E. and Alan, “Akdemir. Some new integral inequalities associated with generalized proportional fractional operators,” Numerical Methods for Partial Differential Equations, vol. 38, no. 5, pp. 1149-1161, Sep. 2022. DOI:10.1002/num.22717.

[7] Q. Nguyen, S. Milani, and H. Marzbani, “Tire-Road Separation Time Reduction by an Adaptive Proportional-Integral-Derivative Controller Utilizing Particle Swarm Optimization Algorithm,” SAE International Journal of Commercial Vehicles, vol. 15, no. 14, pp. 37-50, Oct. 2021. DOI:10.4271/02-14-04-0033.

[8] H. Ding, Y. Huang, J. Shi, and Q. Shi, “Y Yang. A novel industrial AGV control strategy based on dual-wheel chassis model,” Assembly Automation, vol. 42, no. 3, pp. 306-318, Aug. 2022. DOI:10.1108/AA-09-2021-0122.

[9] N. Wang, B. Cai, X. Chu, and B. Su, “Research on suspension control strategy based on finite control set model predictive control with state feedback control-PID for maglev yaw system of wind turbine,” IET Electric Power Applications, vol. 15, no. 2, pp. 255-270, Jan. 2021. DOI:10.1049/elp2.12015.

[10] D. Liu, F. Chang, H. Zhang, L, “Liu. Level set method with Retinex-corrected saliency embedded for image segmentation,” IET Image Processing, vol. 15, no. 7, pp. 1530-1541, Mar. 2021. DOI:10.1049/ipr2.12123.

[11] L. Liu, H. Liu, X. Liu, J. Ma, and M. Xie, “Numerical Simulation of n-Heptane Spray Combustion in a Porous Medium Burner,” Combustion Science and Technology, vol. 195, no. 2, pp. 313-334, Apr. 2023. DOI:10.1080/00102202.2021.1950700.

[12] I. Mohammadi, J. Esfahani, and K. Kim, “A study of the local entropy generation rate in a porous media burner,” Archives of Mechanics, vol. 72, no. 3, pp. 257-279, Oct. 2020. DOI:103.732029/AN.1443.66770.

[13] M. Omidi, Mohsen, D. Emami, “Experimental investigation of premixed combustion and thermal efficiency in a porous heating burner,” International Journal of Energy Research, vol. 45, no. 2, pp. 1948-1958, Jan. 2021. DOI:10.1002/er.5880.

[14] B. Falodun, and A. Omowaye, “Double-diffusive MHD convective flow of heat and mass transfer over a stretching sheet embedded in a thermally-stratified porous medium,” World Journal of Engineering, vol. 16, no. 6, pp. 712-724, Apr. 2019. DOI:10.1108/WJE-09-2018-0306.

[15] S. Devi, N. Sahoo, and P. Muthukumar, “Experimental studies on biogas combustion in a novel double layer inert Porous Radiant Burner,” Renewable Energy, vol. 149, no. Apr., pp. 1040-1052, Apr. 2020. DOI:10.1016/j.renene.2019.10.092.

[16] S. Oslund, C. Washington, A. So, T. Chen, and H. Ji, “Multiview Robust Adversarial Stickers for Arbitrary Objects in the Physical World,” Journal of Computational and Cognitive

Engineering., vol. 1, no. 4, pp. 152-158, January. 2022. DOI:10.47852/bonviewJCCE2022010105.

[17] F. Wang, and L. He, “FPGA-based predictive speed control for PMSM system using integral sliding-mode disturbance observer,” IEEE Transactions on Industrial Electronics, vol. 68, no. 2, pp. 972-981, May. 2020. DOI:10.1109/tie.2020.2969107.

[18] T. Tsai, C. Chang, S. Chen, and C. Yao, “Design of vision-based indoor positioning based on embedded system,” IET Image Processing, vol. 14, no. 3, pp. 423-430, Jan. 2020. DOI:10.1049/iet-ipr.2018.6285.

[19] H. Dai, B. Zhang, Z. Li, and J. Wu, “Combustion characteristics of a porous media burner with partial hydrogen injection,” International Journal of Hydrogen Energy, vol. 47, no. 2, pp. 1092-1102, Feb. 2022. DOI:10.1016/j.ijhydene.2021.10.042.

[20] W. Pakdee, and S. Klayborworn, “Numerical analysis of turbulent non-premixed combustion of syngas and air in a round-jet porous burner,” Journal of Porous Media, vol. 24, no. 4, pp. 55-71, Apr. 2021. DOI:10.1615/JPorMedia.2021025873.